Multifunctional Graphene–PEDOT Microelectrodes for On-Chip Manipulation of Human Mesenchymal Stem Cells

*Yu-Sheng Hsiao, Chiung-Wen Kuo, and Peilin Chen**

All-solution-processed multifunctional organic bioelectronics composed of reduced graphene oxide (rGO) and dexamethasone 21-phosphate disodium salt (DEX)-loaded poly(3,4-ethylenedioxythiophene) (PEDOT) microelectrode arrays on indium tin oxide glass are reported. They can be used to manipulate the differentiation of human mesenchymal stem cells (hMSCs). In the devices, the rGO material functions as an adhesive coating to promote the adhesion and alignment of hMSC cells and to accelerate their osteogenic differentiation. The poly(L-lysine-*graft*-ethylene glycol) (PLL-*g*-PEG)-coated PEDOT electrodes serve as electroactive drug-releasing electrodes. In addition, the corresponding three-zone parallel devices operate as efficient drug-releasing components through spatial-temporal control of the release of the drug DEX from the PEDOT matrix. Such devices can be used for long-term cell culturing and controlled differentiation of hMSCs through electrical stimulation.

1. Introduction

Bone-marrow-derived human mesenchymal stem cells (hMSCs) are multipotent progenitor cells that are capable of differentiating into different cell lineages, including osteoblasts, adipocytes, chondrocytes, and neurons. Controlling the differentiation of hMSCs is one of the most exciting aspects of tissue regeneration therapeutics.[1–3] Much progress has been made in the use of extracellular stimuli, including both physical and chemical cues, to regulate the differentiation of hMSCs. For example, physical cues, such as the mechanical properties of the extracellular matrix[4,5] and the electrical potential of the extracellular environment,[6,7] have been varied to mediate the differentiation of hMSCs into specific osteogenic and/or adipogenic lineages; chemical cues, such as selective-chemical surfaces[8–10] and small-molecule drugs,[11,12] have been employed to regulate cell behavior through control of the extracellular matrix (ECM). Using these approaches, it is possible to manipulate the cell behavior of hMSCs on chips in defined extracellular environments.

Bioelectronic interfaces, potentially bridging the communication gap between biology and electronics, are used widely to enhance the readout performance of biological events in the form of electronic signals and to promote gene expression and biological phenotypes through electrical stimulation (ES).[13–15] Moreover, chemical and topographic design of bioelectronic interfaces can be used to regulate cell behavior, including adhesion, spreading, proliferation, and differentiation.[16–20] By combining contact attraction and repulsion coatings on bioelectronic interfaces, the behavior of cells can be manipulated in both space and time through ES. Therefore, electrically responsive biocompatible interfaces have great potential in a variety of bioelectronic applications, including electrical signaling,[21–23] stimulating,[24–27] and controlled drug release devices.[28–30] In the development of bioelectronic interfaces, two classes of materials: i) conducting polymers [CPs; e.g., polypyrrole (PPy), poly(3,4-ethylenedioxythiophene) (PEDOT)] with a diverse array of anionic dopants [e.g., poly(sodium styrene sulfonate) (PSS), tosylate, (dodecylbenzenesulfonate) (DBS)][13,15,26,31,32] and ii) carbon materials [CMs; e.g., carbon nanotubes, graphene],[27,31,33–38] are often used as biocompatible interfaces for preparing tissue–electrode and cell–electrode interfaces in developmental biology and cell therapies. The electrical, electrochemical, and surface properties of CPs are, however, quite different from those of CMs. For example, CPs and CMs are hole and electron transporting materials, respectively; the redox capabilities of thin films of CPs are higher than those of CMs; and anion-doped CPs and unfunctionalized CMs present negatively charged and neutral surfaces, respectively. Notably, the solution-processable reduced graphene oxide (rGO) is a promising CM, that has the potential to mediate the molecule and gene expression levels in various cell types, including neurons, fibroblasts, osteoblasts, etc.[27,35,37,38] Because the facile solution-processes for preparing CPs and rGO materials are compatible in thin film fabrication, it is possible to design optoelectronic devices incorporating both materials to obtain functions that cannot be performed by the individual materials.

In this paper we describe a multifunctional bioelectronic interface, composed of rGO and dexamethasone 21-phosphate disodium salt (DEX)-loaded PEDOT microelectrode arrays on indium tin oxide glass, that takes advantage of the individual properties of the CM and the CP. Because of the efficient anti-adhesive coating of poly(L-lysine-*graft*-ethylene glycol) (PLL-*g*-PEG) on PEDOT surfaces and the DEX-condensing behavior

Dr. Y.-S. Hsiao, Dr. C.-W. Kuo, Dr. P. Chen
Research Center for Applied Sciences
Academia Sinica, Taipei 11529, Taiwan
E-mail: peilin@gate.sinica.edu.tw

DOI: 10.1002/adfm.201203631

of rGO surfaces,[27,37] this rGO–PEDOT microarray device can be used to manipulate the location and differentiation of hMSCs on chips and electrically activate the release of the drug for long-term osteogenic differentiation.

2. Results and Discussion

2.1. Electrical Characteristics of PEDOT and rGO Materials

To assess the electrochemical properties of PEDOT and rGO materials for use in bioelectronic interfaces, we used cyclic voltammetry (CV; voltage swept from –0.9 to 0.5 V) to explore the charge capacity density (CCD) of PEDOT- and rGO-coated ITO electrodes in phosphate-buffered saline (PBS, 0.1 M, pH 7.2) (**Figure 1**a). The higher CCD of PEDOT (4.22 mC cm^{-2}) indicates that it is capable of more-efficient drug loading and release, relative to that measured for the rGO electrode (0.58 mC cm^{-2}). In addition, we used electrochemical impedance spectroscopy to measure the ionic conductivity in the frequency range from 1 to 10^5 Hz (Figure 1b). The impedance of PEDOT at 1 Hz was approximately two orders of magnitude lower that that of the bare ITO and rGO/ITO electrodes in PBS (0.1 M, pH 7.2), indicating that the PEDOT would readily undergo ionic exchange during the cyclic potential ES. Therefore, we expected an integrated rGO–PEDOT bioelectronic interface to exhibit high electrical stability toward cells on the rGO electrodes, while its PEDOT electrodes would function as an efficient electrically modulated drug release system.

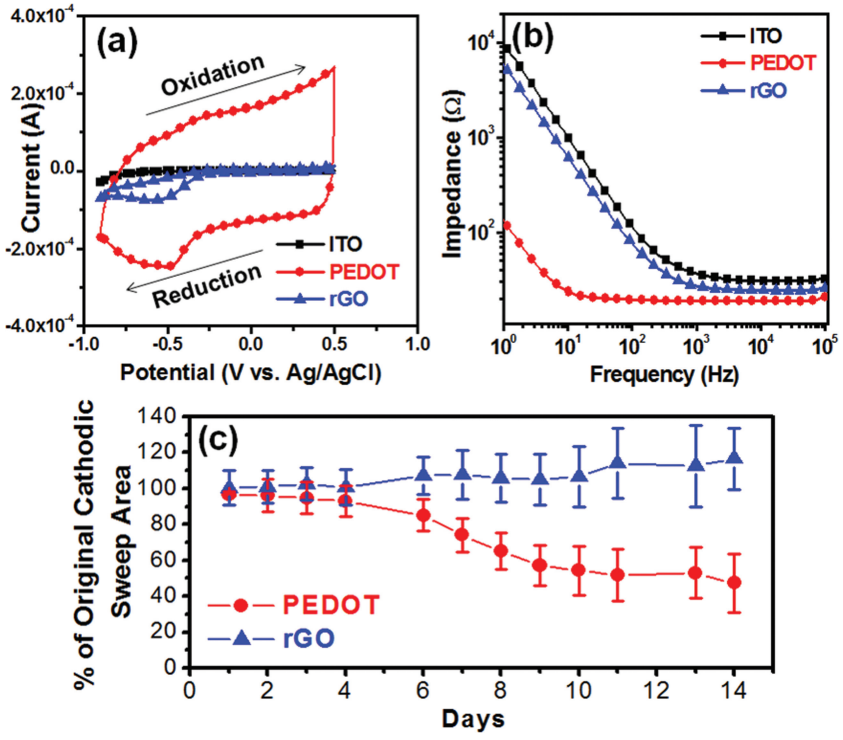

Figure 1. Electrical properties of various bioelectronic interfaces on ITO glass. a) CV: Potential swept from –0.9 to 0.5 V at a scan rate of 100 mV s^{-1}. CCDs for ITO, PEDOT:PSS, and rGO were 0.07, 4.22, and 0.58 mC cm^{-2}, respectively. b) Electrochemical impedance spectroscopy (frequency range, 1–10^5 Hz). c) Decline of electroactivity in PBS (1×).

2.2. DEX Drug Effect on hMSCs

To determine the effect of the drug DEX on the osteogenic differentiation of hMSCs, we used electric cell–substrate impedance sensing (ECIS) to monitor the long-term changes in the cell membrane properties as well as the degree of osteogenic differentiation of the hMSCs. **Figure 2**a presents the time-course measurement of the mean impedance of the hMSCs, at 16 kHz, over 12 days for four groups ($n = 3$): no cell control, cells under the growth medium, cells under osteogenesis induction medium without DEX, and cells under osteogenesis induction medium with DEX. Although replacement of the medium every 3 days created some artificial peaks in the impedance spectra (as a result of slight changes in pH, temperature, and dissolved CO_2[39]), the trends in impedance were clearly evident after induction for approximately 50 h. No features appeared in the impedance spectra for the no-cell group; in contrast, the growth medium–only group promoted cell proliferation, resulting in a steady increase in the first 6 days of cultivation, reaching a plateau of approximately 300 Ω during the 6–12 day period. The osteogenesis induction medium without DEX group exhibited cell confluency and detachment responses,[39] thereby causing the impedance spectra to level off after 12 days of long-term cultivation. When DEX was added to the osteogenesis induction medium in the cell culture, however, the membrane potential increased rapidly, as evidenced by the impedance spectra over the course of differentiation toward the osteogenic lineage during the 3–9 days, reaching a plateau of approximately 600 Ω after 12 days. In addition, we used the alkaline phosphatase (ALP) assay to directly evaluate the differentiation status of the hMSCs at the end of the ECIS experiments (Figure 2b–d). Comparing the results from previous studies[39–41] with our results for ALP expression in the osteogenesis induction medium with and without DEX in the growth medium, the drug appears to play an important role in signaling the osteogenic differentiation. Therefore, we selected a 9-day period of osteogenesis induction with DEX as the drug model to further investigate the manipulation of hMSCs and controlled drug release induced by our rGO–PEDOT microelectrode arrays.

2.3. Accelerating Osteogenic Differentiation of hMSCs on rGO

Recently, it has been demonstrated by many groups that graphene is a candidate material for accelerating gene expression and osteogenic differentiation.[34,36,37] To evaluate

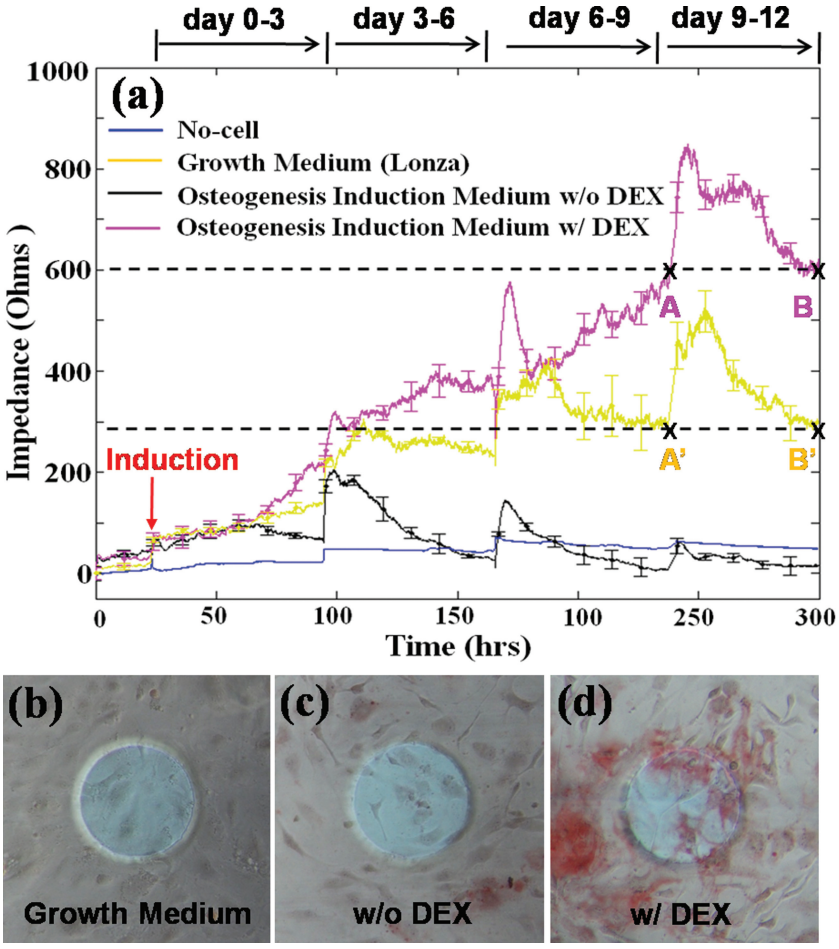

Figure 2. a) Cell culture medium and drug screening for hMSCs using ECIS chips. b–d) ALP analyses of hMSCs after 12 days in various induction media: b) growth medium, c) osteogenesis induction medium in the absence of DEX, and d) osteogenesis induction medium in the presence of DEX.

the conversion of hMSCs to the rGO electrodes, we used two immunofluorescent staining markers, CD-44–positive and osteocalcin (OCN)-negative markers, to stain the hMSCs at different periods of time (0, 3, 6, and 9 days) during osteogenesis induction. The progressive decrease in the CD-44 fluorescence intensity and enhanced OCN fluorescence (**Figure 3**) confirmed the successful osteogenic differentiation on the rGO/ITO electrodes after 9 days of induction. In addition, the hMSCs became more spread out and larger after 3 days of incubation.

To confirm that the rGO electrodes of our devices could accelerate hMSC differentiation into the osteogenic lineage, we recorded light microscopy images of rGO/ITO electrodes with hMSCs on tissue culture polystyrene (TCPS) dishes that had been subjected to Alizarin Red S staining after 3, 6, and 9 days of osteogenesis induction in the presence of the drug DEX. **Figure 4**a–f reveal a higher differentiation potential toward the osteogenic lineage for the hMSCs on the rGO surfaces than those on the TCPS dishes at day 9 of induction. Notably, more of the hMSCs growing on the rGO electrodes could develop into osteoblast-like cells with the formation of the mineralized nodule (Figure 4f,g). To precisely quantify the osteogenic differentiation potential of hMSCs on our rGO surfaces in the presence of DEX, we used the red color of the calcium deposits to further analyze the cell percentage of ALP coverage (Figure 4h). In a result similar to that of our ECIS study, the ALP expression of the hMSCs on the rGO/ITO surfaces exhibited an impressive osteogenic differentiation potential after a 9-day period of osteogenesis induction in the presence of DEX.

2.4. rGO–PEDOT Devices for Manipulating hMSCs Behavior

To test the on-chip concept for manipulating stem cells and controlling drug release through ES, we used DEX as the drug model to develop an organic bioelectronic platform (rGO–PEDOT) with alternating microelectrode arrays of rGO and DEX-loaded PEDOT (**Figure 5**). The rGO–PEDOT microelectrodes of different sizes (rGO–PEDOT-20, rGO–PEDOT-50, rGO–PEDOT-100; the numbers indicate width in micrometers) were patterned through photolithography and subsequent electrical polymerization of the PEDOT materials (Figure 5a–f).[27] The attenuated total reflection Fourier transform infrared (ATR-FTIR) spectra in Figure S1 (Supporting Information) confirmed that DEX could be loaded into the PEDOT films during the polymerization process.

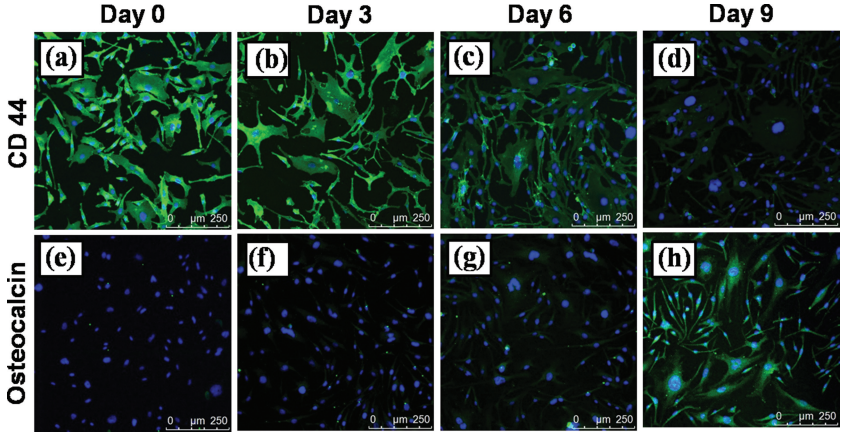

Figure 3. Immunofluorescence staining of hMSCs grown on rGO-coated ITO substrates for 0, 3, 6, and 9 days of osteogenesis induction. a–d) CD44, marker for undifferentiated stem cells; e–h) osteocalcin, marker for bone cells.

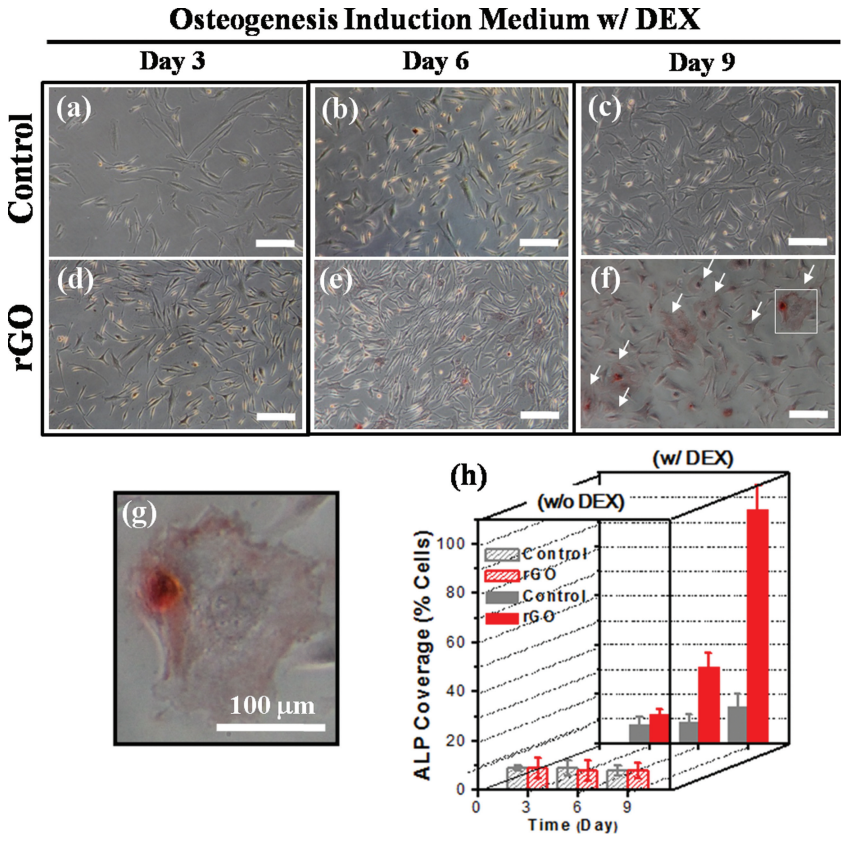

Figure 4. a–f) Immunohistochemical staining of hMSCs grown on TCPS dishes (control) and rGO-coated ITO substrates for 3, 6, and 9 days of osteogenesis induction. Scale bar: 200 μm. g) Morphological analysis of mineralized nodule formation of hMSCs. h) Quantification of ALP expression through Alizarin Red staining of hMSCs differentiated on various substrates.

To test the drug release capability, we fabricated rGO–PEDOT architectures (Devices 1–3) (Figure 5g–i) featuring three different coating schemes: no coating was applied in Device 1, a poly(3,4-ethylenedioxythiophene):polystyrenesulfonate (PEDOT:PSS) blocking layer was added in Device 2, and an additional anti-adhesive coating of PLL-*g*-PEG was used in Device 3. The drug releasing capabilities of the three different rGO–PEDOT electrodes were activated by a cyclic potential ES with the voltage swept from–1 to +1 V at a scan rate of 100 mV s^{-1} for *n* cycles in PBS (1×). **Figure 6**a presents the DEX release profiles of Devices 1–3 in PBS (1×) solution, as measured at 242 nm using UV spectroscopy. As expected, in the absence of the PEDOT:PSS blocking layer on the PEDOT:DEX surfaces (Device 1), a significant amount of DEX was released from the rGO–PEDOT microelectrode arrays in the absence of ES, due to diffusion. When a blocking layer of PEDOT:PSS was present on top of the PEDOT:DEX layers, however, the DEX molecules were sealed very well in Devices 2 and 3 in the absence of ES; upon ES, DEX was released linearly over time in these devices, due to the swelling/deswelling kinetics of the conducting polymeric materials.[28,42,43] Figure 6b illustrates the long-term DEX release profile of Device 3 in PBS solution, where almost no DEX was released without ES. Upon ES, approximately 19 μg cm^{-2} of DEX were released from our device after incubation for 6 days. With the aim of applying this electrically responsive drug release system to the osteogenic differentiation of hMSCs, we further optimized the DEX-loaded rGO–PEDOT microelectrode arrays into three-zone parallel devices (ES1–3) that could provide drug release at three different time points during the osteogenesis induction period (Figure 6b, inset). Figure 6c reveals that the rGO–PEDOT device provided the system with a fresh dose of DEX released every 3 days for 9 days in vitro (DIV). Notably, the cyclic potential method not only provides the controlled release of DEX but also preserves the anti-adhesion performance of PLL-*g*-PEG during ES, thereby maintaining the attachment of hMSCs onto the rGO strips (Figure 6d).

When using hMSCs in tissue regeneration therapy, the attachment, alignment, and spatial organization of the hMSCs are entirely responsible for guiding tissue generation through long-term induction of the differentiation process. Therefore, it is desirable to control the alignment of the hMSCs on chips. Accordingly, we tested rGO–PEDOT microelectrode arrays of various sizes for their ability to spatially manipulate the location and spreading orientations of the hMSCs at 6 DIV in the growth medium (**Figure 7**). The large widths of the rGO–PEDOT-100 electrodes effectively prevented the hMSCs from spreading over two neighboring electrodes, as evidenced by the efficient anti-adhesive coating of the FITC-labeled PLL-*g*-PEG on the PEDOT stripes (Figure 7a–d). Furthermore, the cell-orientation distributions of the hMSCs, obtained using Image J software and summarized in Figure 7e for the differently sized rGO–PEDOT devices (300 cells measured in each case), revealed that the narrow electrodes in the rGO–PEDOT-50 and rGO–PEDOT-20 devices provided better control over the alignment of the hMSCs along the direction of the stripes, with approximately 95% of the cells oriented at angles of less than 40°.

To demonstrate the potential application of our rGO-PEDOT electrode system in stem cell therapy, we used the optimized three-zone parallel device (**Device 3**) to study the long-term cell alignment stability and osteogenic induction for hMSCs (**Figure 8**a–e). During the 9-day period of osteogenic induction, three doses of DEX drugs were released from the differently sized rGO–PEDOT devices under ES, thereby inducing osteocalcin expression (immunofluorescence image; green) in the hMSCs and eventually leading to formation of bone matrix nodules.[36,37] Furthermore, Figure 8a–d reveal that the anti-adhesive coating, which we used to guide cell attachment and orientation, on our devices survived the long-term incubation with hMSCs on the rGO–PEDOT-20 devices, presumably because of confluence and physical constriction of the hMSCs on the small adhesive microelectrode arrays as a result of cell crowding.[44,45] As expected, the larger rGO–PEDOT-100 device could up-regulate osteocalcin expression on the rGO stripes, as

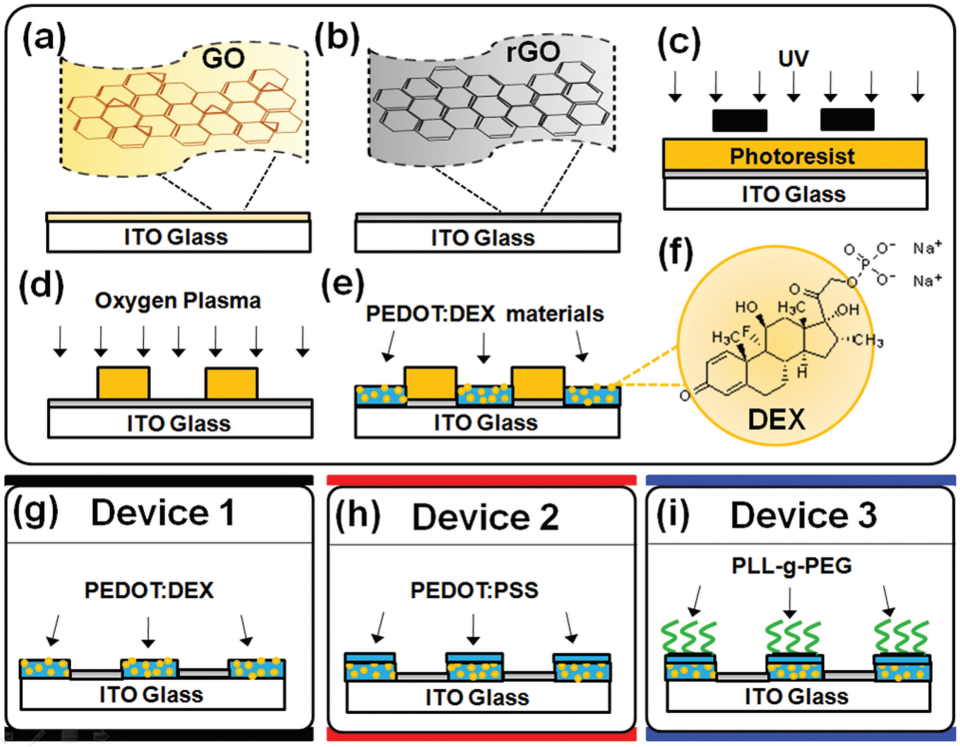

Figure 5. a–f) Schematic representation of the fabrication of DEX-loaded organic bioelectronics featuring alternating microelectrode arrays. g–i) Architectures of DEX-loaded organic bioelectronics: g) Device 1, rGO-PEDOT device; h) Device 2, Device 1 with PEDOT:PSS blocking layers; and i) Device 3, Device 2 with anti-adhesive coatings of PLL-*g*-PEG.

indicated by the arrows in Figure 8e. Comparing our present results with those in previous reports,[27,28,36,37,44,45] it is evident that some important bioelectronic features can be integrated into our rGO–PEDOT devices (Figure 8f): i) the optimized device architecture of the DEX-loaded PEDOT can serve as a drug release component under electrical modulation; ii) the rGO electrodes have the ability to preconcentrate the drug DEX on their surfaces to enhance the cell endocytic process; iii) rGO microelectrode arrays featuring optimized dimensions can increase the degree of osteogenic expression in hMSCs; and iv) PLL-*g*-PEG–coated PEDOT microelectrode arrays can be used as an efficient means of regulating cell spreading morphologies on rGO surfaces.

3. Conclusions

We have constructed a multifunctional rGO–PEDOT bioelectronic interface for manipulating the attachment and orientation of hMSCs; we further integrated this device with a drug releasing model to up-regulate the osteogenic differentiation of hMSCs under electrical modulation. Adding an anti-adhesive coating of PLL-*g*-PEG onto the PEDOT microelectrode arrays allowed us to organize the cells onto rGO stripes, extend the electrochemical behavior of the PEDOT material toward long-term drug release, and facilitate the drug preconcentration and delivery performance of the graphene material, thereby accelerating the osteogenic differentiation of hMSCs. Furthermore, we explored the effect of the dimensions of the rGO–PEDOT microelectrode arrays on the cell spreading and expression of differentiation; whereas the smaller rGO–PEDOT-20 array exhibited better cell alignment ability, the larger rGO–PEDOT-100 exhibited better performance at inducing osteocalcin expression in hMSCs. We also found that using three-zone parallel devices made it possible to release drugs at three points in time. This concept could presumably be extended to release different types of drugs at different lineages on defined patterns. Eventually, such devices might be applicable in tissue engineering and regenerative medicine.

4. Experimental Section

Device Fabrication with Alternating rGO–PEDOT Microelectrode Arrays: Figure 5a–e presents a schematic representation of the fabrication of rGO-PEDOT microelectrode arrays; this procedure was identical to that described previous reports.[27,46] Briefly, GO was first synthesized based on a modified version of Hummers method.[47] A large-scale rGO-coated ITO glass was then obtained after spin-coating of the fully exfoliated GO aqueous dispersion and subsequent chemical reduction in hydrazine vapor at 60 °C for 6 h. A standard photolithography process, with positive resist (S-1813, Shipley) and development (MF-319, Shipley), was used to fabricate S-1813 microarray patterns of three different sizes (100, 50, and 20 μm) on the rGO-coated ITO glass; the patterns were then subjected to oxygen plasma treatment to remove the opening area of the rGO from the ITO surface. Thin PEDOT layers were then deposited electrochemically on ITO from a bath aqueous

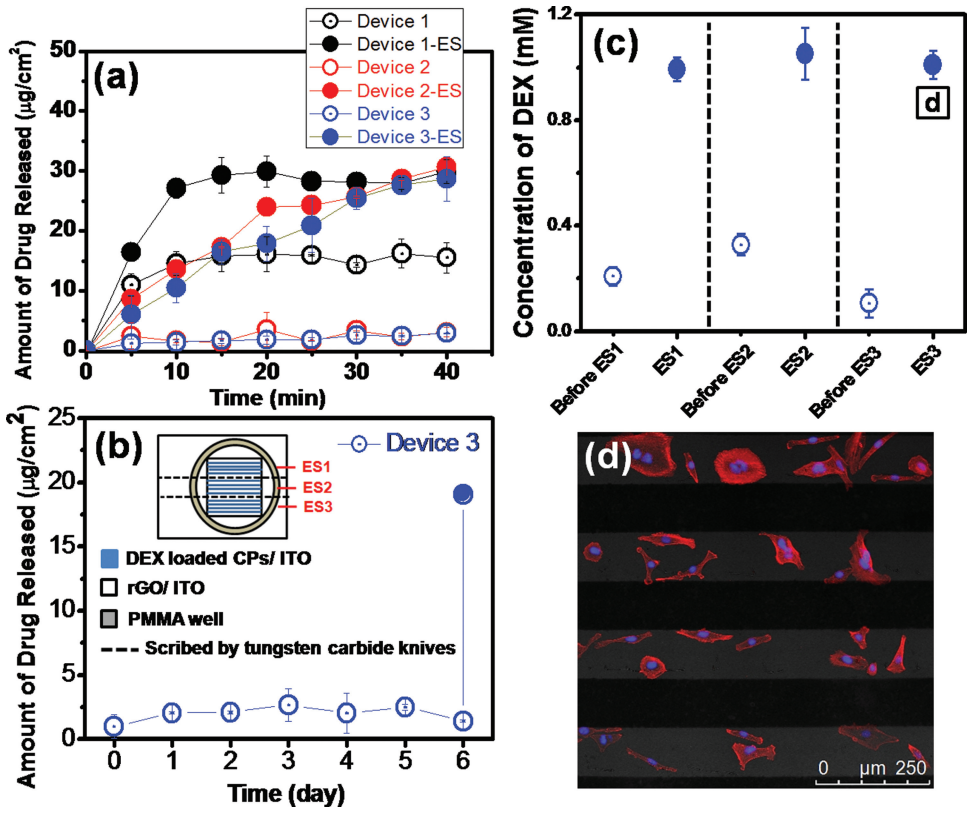

Figure 6. a) Time-dependent DEX release profiles from rGO–PEDOT-100 microelectrode array devices. The release of DEX (n = 5) in PBS (1×) with and without ES was detected at 242 nm using UV–Vis spectroscopy. b) Long-term stability of the electrically triggered DEX release from Device 3 in the incubator at 37 °C. Inset: Schematic representation of Device 3 with three zones of ES. c) Final DEX concentration after the individual electrically modulated drug release from the three zones of ES. Prior to ES, PBS (1×) was replaced with fresh buffer; the DEX concentration was measured 40 min after changing the PBS. d) hMSC spreading morphologies on Device 3 after three cycles of ES and 1 day of incubation, as revealed by F-actin (red) for the cytoskeleton and DAPI (blue) for the nucleus.

solution containing 0.01 M 3,4-ethylenedioxythiophene (EDOT; Sigma–Aldrich), 0.01 M DEX (Sigma–Aldrich), 10% (w/v) PEG (M_n = 20 000) and/or anionic poly(sodium 4-styrenesulfonate) (PSS, M_n = 70 000, 2 wt%; Sigma–Aldrich) using the three-electrode system of an Autolab PGSTAT-12 electrochemical analyzer (EcoChemie, Utrecht, Netherlands). A constant potential of 1 V (vs. Ag/Ag^+) was used to produce PEDOT:DEX and PEDOT:PSS layers with a range of deposition densities (10–20 mC cm^{-2}). The S-1813 photoresist was removed by washing with acetone, leaving the surfaces of the ITO glasses covered with rGO–PEDOT microelectrode arrays (rGO–PEDOT). PLL-*g*-PEG (Surface Solution, Switzerland) was used to modify the PEDOT surface of rGO–PEDOT for 1 h, resulting in a contact repulsion surface that prevented cell seeding in the first growth phase. The PLL-*g*-PEG solution (0.1 mg mL^{-1}, pH 7.2) was prepared in 10 mM 4-(2-hydroxyethyl)-1-piperazineethanesulfonic acid (HEPES) buffer. Contact repulsion coatings of PLL-*g*-PEG on rGO–PEDOT microelectrode arrays have been described in a previous report.[27]

Electrically Modulated Drug Release: The cyclic potential ES was performed in a two-electrode set-up with the voltage swept from –1 to +1 V at a scan rate of 100 mV s^{-1} for n cycles in PBS (1×). The DEX release was monitored at 242 nm using UV spectroscopy. The calibration curve for DEX in PBS (1×) featured high linearity (R^2 = 0.9993) (Figure S2, Supporting Information). After five CV cycles of ES, UV reading of the PBS (1×) solution was performed five times with a time interval of 5 min. For long-term cell cultures prepared using the rGO–PEDOT devices, 40 CV cycles were applied for each active area of the rGO–PEDOT microelectrode arrays.

Cell Culture: The hMSCs (Neuromics, Edina, MN) used in experiments were at passage 3-9. Each passage of hMSCs was maintained on the TCPS dishes with a pre-coating of Geltrex reduced growth factor basement membrane matrix (Invitrogen, CIBCO, NY). All hMSCs were maintained in the growth medium, Dulbecco's modified Eagle's medium-low glucose (DMEM-LG) supplemented with mesenchymal cell growth supplement (MSCGM, Lonza) containing L-glutamine, penicillin, and streptomycin, and incubated in an atmosphere containing 5% CO_2 at 37 °C. The medium was replenished every 3 to 4 days.

For osteogenic differentiation, the hMSCs were cultured in the osteogenesis induction medium, DMEM-LG supplemented with mesenchymal stem cell osteogenesis kit (Chemicon, Cat. No. SCR028), and incubated on the TCPS dishes (control) and test devices. To study the drug release from the devices, hMSCs were cultured in the osteogenesis induction medium in the absence of DEX. The fresh medium was replaced every 2 to 3 days.

Microscopy and Data Analysis: For measurements of drug release, immunofluorescence staining, and ALP activity, the cell seeding density was 12 000 cells cm^{-2} in each case. After incubation, the differentiated hMSCs were monitored directly through a confocal microscope (Leica TCS SP5) using phase, differential interference contrast (DIC), or fluorescent imaging. Markers (CD44 and osteocalcin) were purchased from Millipore. Alexa Fluor 488 goat anti-mouse IgG (H+L) was purchased from Invitrogen.

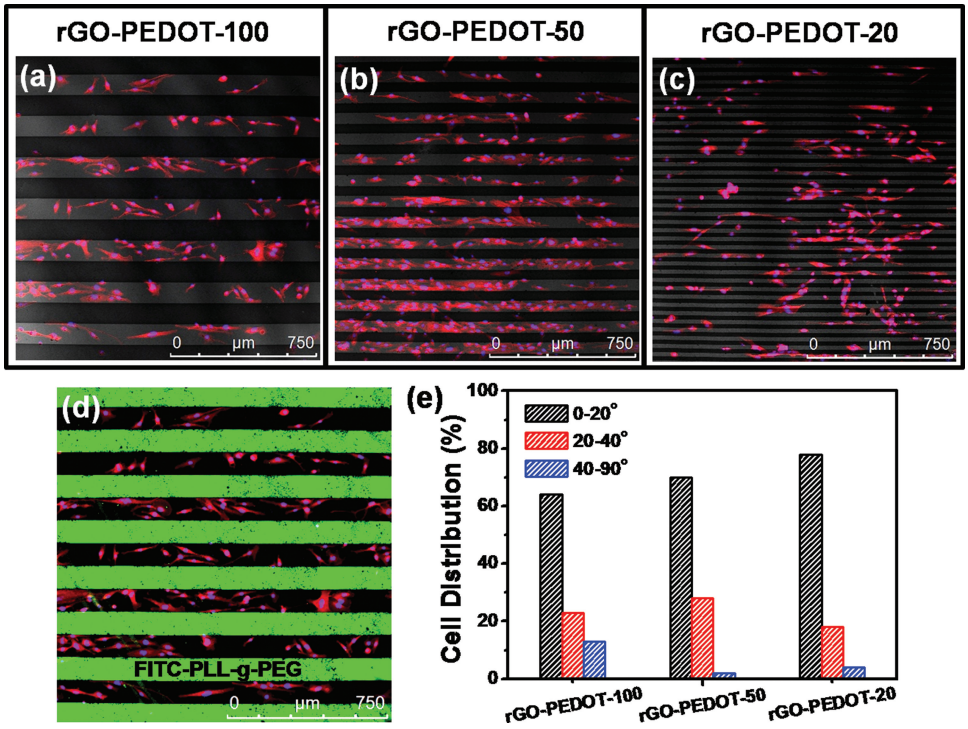

Figure 7. a–c) Immunofluorescence staining of hMSCs grown on rGO–PEDOT microelectrode arrays of various sizes (rGO–PEDOT-100, rGO–PEDOT-50, rGO–PEDOT-20). d) Immunofluorescence staining of hMSCs grown on rGO–PEDOT-100, as evidenced by the anti-adhesive coating of the FITC-labeled PLL-*g*-PEG (green) on the PEDOT stripes. Cells were seeded and cultured for 6 days in growth medium; F-actin (red) revealed the cytoskeleton and DAPI (blue) revealed the nucleus. e) Cell-orientation distributions of hMSCs on rGO–PEDOT microelectrode arrays of various sizes.

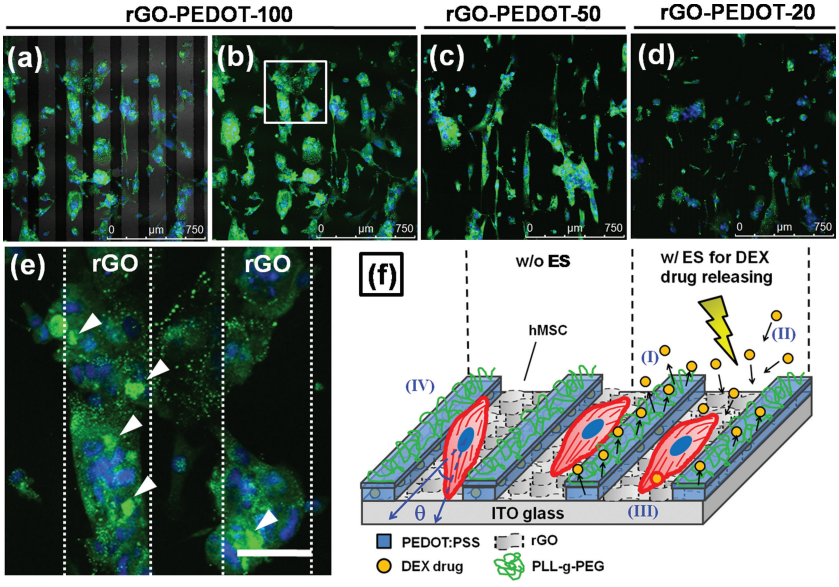

Figure 8. a–d) Osteocalcin expression in hMSCs cultured on rGO–PEDOT microelectrode arrays of various sizes (rGO–PEDOT-20, rGO–PEDOT-50, rGO–PEDOT-100), revealed through immunofluorescence staining. Cells were cultured for 9 days in osteogenesis induction medium in the absence of DEX; drug release was modulated electrically through three cycles of ES (three-day interval); osteocalcin (green) revealed the bone matrix and DAPI (blue) revealed the nucleus. e) Enlarged view of immunofluorescence of osteocalcin expression in hMSCs cultured on rGO–PEDOT-100. Arrows indicated the formation of bone matrix nodules. Scale bar: 100 µm. f) Schematic representation of some bioelectronic features integrated into our rGO–PEDOT devices.

The ALP activity was analyzed using Alizarin Red S staining; Alizarin Red solution was purchased from Chemicon (cat. no. 2004012). Briefly, the medium was aspirated out from each well and then the cells were fixed with ice-cold 70% EtOH for 1 h at room temperature. The cells were rinsed twice with DI water and then each well was covered with Alizarin Red solution (1.5 mL). After 30 min of incubation, the unstained Alizarin Red was washed four times with DI water and then the samples were visualized under an inverted microscope (Leica DMIL).

Supporting Information

Supporting Information is available from the Wiley Online Library or from the author.

Acknowledgements

This study was supported in part by the National Science Council (NSC) of Taiwan under contract NSC 100-2113-M-001-027-MY3, NSC-101-2120-M-001-011 and by the Academia Sinica Research Project on Nano Science and Technology.

Received: December 1, 2012
Published online: April 9, 2013

[1] M. F. Pittenger, A. M. Mackay, S. C. Beck, R. K. Jaiswal, R. Douglas, J. D. Mosca, M. A. Moorman, D. W. Simonetti, S. Craig, D. R. Marshak, *Science* **1999**, *284*, 143.
[2] A. Uccelli, L. Moretta, V. Pistoia, *Nat. Rev. Immunol.* **2008**, *8*, 726.
[3] O. Honmou, R. Onodera, M. Sasaki, S. G. Waxman, J. D. Kocsis, *Trends Mol. Med.* **2012**, *18*, 292.
[4] A. J. Engler, S. Sen, H. L. Sweeney, D. E. Discher, *Cell* **2006**, *126*, 677.
[5] M. T. Yang, J. P. Fu, Y. K. Wang, R. A. Desai, C. S. Chen, *Nat. Protoc.* **2011**, *6*, 187.
[6] S. Sundelacruz, M. Levin, D. L. Kaplan, *PLoS One* **2008**, *3*, e3737.
[7] T. H. Chung, S. H. Wu, M. Yao, C. W. Lu, Y. S. Lin, Y. Hung, C. Y. Mou, Y. C. Chen, D. M. Huang, *Biomaterials* **2007**, *28*, 2959.
[8] J. M. Curran, R. Chen, J. A. Hunt, *Biomaterials* **2006**, *27*, 4783.
[9] D. S. Benoit, M. P. Schwartz, A. R. Durney, K. S. Anseth, *Nat. Mater.* **2008**, *7*, 816.
[10] H. Y. Wang, D. T. K. Kwok, M. Xu, H. G. Shi, Z. W. Wu, W. Zhang, P. K. Chu, *Adv. Mater.* **2012**, *24*, 3315.
[11] M. Sila-Asna, A. Bunyaratvej, S. Maeda, H. Kitaguchi, N. Bunyaratvej, *J. Med. Sci.* **2007**, *53*, 25.
[12] Y. Xiao, V. Peperzak, L. van Rijn, J. Borst, J. D. de Bruijn, *J. Tissue Eng. Regen. Med.* **2010**, *4*, 374.
[13] M. Asplund, T. Nyberg, O. Inganäs, *Polym. Chem.* **2010**, *1*, 1374.
[14] L. Ghasemi-Mobarakeh, M. P. Prabhakaran, M. Morshed, M. H. Nasr-Esfahani, H. Baharvand, S. Kiani, S. S. Al-Deyab, S. Ramakrishna, *J. Tissue Eng. Regen. Med.* **2011**, *5*, e17.
[15] K. Svennersten, K. C. Larsson, M. Berggren, A. Richter-Dahlfors, *Biochim. Biophys. Acta* **2011**, *1810*, 276.
[16] N. Gomez, J. Y. Lee, J. D. Nickels, C. E. Schmidt, *Adv. Funct. Mater.* **2007**, *17*, 1645.
[17] S.-C. Luo, E. M. Ali, N. C. Tansil, H.-h. Yu, S. Gao, E. A. B. Kantchev, J. Y. Ying, *Langmuir* **2008**, *24*, 8071.
[18] S.-C. Luo, S. S. Liour, H.-h. Yu, *Chem. Commun.* **2010**, *46*, 4731.
[19] J. Sekine, S.-C. Luo, S. Wang, B. Zhu, H.-R. Tseng, H.-h. Yu, *Adv. Mater.* **2011**, *23*, 4788.
[20] S.-C. Luo, B. Zhu, A. Nakao, R. Nakatomi, H.-h. Yu, *Adv. Eng. Mater.* **2011**, *13*, B423.
[21] D. T. Simon, S. Kurup, K. C. Larsson, R. Hori, K. Tybrandt, M. Goiny, E. H. Jager, M. Berggren, B. Canlon, A. Richter-Dahlfors, *Nat. Mater.* **2009**, *8*, 742.
[22] D.-H. Kim, J. A. Wiler, D. J. Anderson, D. R. Kipke, D. C. Martin, *Acta Biomater.* **2010**, *6*, 57.
[23] S. Y. Yang, B. N. Kim, A. A. Zakhidov, P. G. Taylor, J. K. Lee, C. K. Ober, M. Lindau, G. G. Malliaras, *Adv. Mater.* **2011**, *23*, H184.
[24] J. Xie, M. R. MacEwan, S. M. Willerth, X. Li, D. W. Moran, S. E. Sakiyama-Elbert, Y. Xia, *Adv. Mater.* **2009**, *19*, 2312.
[25] A. F. Quigley, J. M. Razal, B. C. Thompson, S. E. Moulton, M. Kita, E. L. Kennedy, G. M. Clark, G. G. Wallace, R. M. I. Kapsa, *Adv. Mater.* **2009**, *21*, 4393.
[26] Y.-S. Hsiao, C.-C. Lin, H.-J. Hsieh, S.-M. Tsai, C.-W. Kuo, C.-W. Chu, P. Chen, *Lab Chip* **2011**, *11*, 3674.
[27] C.-H. Lu, Y.-S. Hsiao, C.-W. Kuo, P. Chen, *Biochim. Biophys. Acta* **2012**, DOI: 10.1016/j.bbagen.2012.08.028.
[28] R. Wadhwa, C. F. Lagenaur, X. T. Cui, *J. Controlled Release* **2006**, *110*, 531.
[29] M. R. Abidian, D. C. Martin, *Adv. Funct. Mater.* **2009**, *19*, 573.
[30] J. Ge, E. Neofytou, T. J. Cahill, R. E. Beygui, R. N. Zare, *ACS Nano* **2011**, *6*, 227.
[31] L. Ghasemi-Mobarakeh, M. P. Prabhakaran, M. Morshed, M. H. Nasr-Esfahani, H. Baharvand, S. Kiani, S. S. Al-Deyab, S. Ramakrishna, *J. Tissue Eng. Regen. Med.* **2011**, *5*, e17.
[32] D. C. Martin, J. H. Wu, C. M. Shaw, Z. King, S. A. Spanninga, S. Richardson-Burns, J. Hendricks, J. Y. Yang, *Polym. Rev.* **2010**, *50*, 340.
[33] G. Cellot, E. Cilia, S. Cipollone, V. Rancic, A. Sucapane, S. Giordani, L. Gambazzi, H. Markram, M. Grandolfo, D. Scaini, F. Gelain, L. Casalis, M. Prato, M. Giugliano, L. Ballerini, *Nat. Nanotechnol.* **2009**, *4*, 126.
[34] S.-R. Ryoo, Y.-K. Kim, M.-H. Kim, D.-H. Min, *ACS Nano* **2010**, *4*, 6587.
[35] D. W. Lin, C. J. Bettinger, J. P. Ferreira, C. L. Wang, Z. Bao, *ACS Nano* **2011**, *5*, 10026.
[36] T. R. Nayak, H. Andersen, V. S. Makam, C. Khaw, S. Bae, X. Xu, P. R. Ee, J. H.Ahn, B. H. Hong, G. Pastorin, B. Özyilmaz, *ACS Nano* **2011**, *5*, 4670.
[37] W. C. Lee, C. Lim, H. Shi, L. A. L. Tang, Y. Wang, C. T. Lim, K. P. Loh, *ACS Nano* **2011**, *5*, 7334.
[38] C. Schmidt, *Nature* **2011**, *483*, S37.
[39] P. O. Bagnaninchi, N. Drummond, *Proc. Natl. Acad. Sci. USA* **2011**, *108*, 6462.
[40] K. Hanada, J. E. Dennis, A. I. Caplan, *J. Bone Miner. Res.* **1997**, *12*, 1606.
[41] Z. Hamidouche, O. Fromigué, J. Ringe, T. Häupl, P. Vaudin, J.-C. Pagès, S. Srouji, E. Livne, P. J. Marie, *Proc. Natl. Acad. Sci. USA* **2009**, *106*, 18587.
[42] J.-M. Pernaut, *J. Phys. Chem. B* **2000**, *104*, 4080.
[43] G. Jeon, S. Y. Yang, J. K. Kim, *J. Mater. Chem.* **2012**, *22*, 14814.
[44] S. A. Ruiz, C. S. Chen, *Stem Cells* **2008**, *26*, 2921.
[45] Y.-K. Wang, X. Yu, D. M. Cohen, M. A. Wozniak, M. T. Yang, L. Gao, J. Eyckmans, C. S. Chen, *Stem Cells Dev.* **2012**, *21*, 1176.
[46] K.-J. Huang, Y.-S. Hsiao, J.-H. Huang, C.-W. Chu, P. Chen, W.-T. Whang, *J. Mater. Chem.* **2012**, *22*, 7837.
[47] W. S. Hummers, R. E. Offeman, *J. Am. Chem. Soc.* **1958**, *80*, 1339.